J. Fluid Mech. (1986), *vol.* 162, *pp.* 139–156
Printed in Great Britain

On the time development of meander bends

By GARY PARKER

St Anthony Falls Hydraulic Laboratory, University of Minnesota, Minneapolis, Minnesota 55414

AND EDMUND D. ANDREWS

US Geological Survey, Lakewood, Colorado 80225

(Received 2 March 1984 and in revised form 15 July 1985)

According to the theory of Ikeda, Parker & Sawai (1981), meander migration rate at a point depends on a convolution integral of channel curvature from that point upstream. The problem can be quantified in terms of the bend equation. The time development of periodic bend trains of finite amplitude is analysed using the method of two-timing. The results apply near the critical wavenumber for the growth of bends of infinitesimal amplitude.

A finite-amplitude equilibrium state bifurcating from the null state at the critical wavenumber was delineated by Parker, Diplas & Akiyama (1983): they called the resulting solution the Kinoshita curve. It is found herein that this equilibrium state is unstable. Bends of longer Cartesian wavelength grow to cutoff. Shorter bends are obliterated. Nevertheless, in either case, the bend train tends towards the shape of the Kinoshita curve.

The theory suggests that some growing bends may be stabilized by local obstructions to downstream migration. The obstructions would cause an effective reduction in Cartesian wavelength, moving the bend from the unstable regime to the stable regime. A rather crude check of bend shape and rates of deformation generally lends support to the analysis.

1. Introduction

The shape and deformation of finite-amplitude meander bends have been the subject of much speculation, but have only recently yielded to analytical treatment. Ikeda, Parker & Sawai (1981) coupled Engelund's (1974) theory of flow in bends with a kinematic treatment of bank erosion in order to delineate the bend equation, a nonlinear equation describing the deformation of meander trains. They performed a linear stability analysis, and delineated a critical wavenumber above which bends are stable, and below which bends are unstable. They also determined a characteristic wavenumber of maximum instability. Similar linear analyses have been performed by Kitanidis & Kennedy (1984) and Blondeaux & Seminara (1985).

Parker, Sawai & Ikeda (1982) used an expansion in amplitude to study nonlinear effects on bend growth and deformation. They found that, as amplitude increases, the initial downstream migration rate declines. A periodic bend train was found to develop a characteristic skewing, or asymmetry, that is commonly seen in nature (Kinoshita 1961; Carson & Lapointe 1983). This asymmetry can be seen in figure 1. The nonlinear analysis, however, is not valid for a greater time period than that of the linear analysis.

Parker, Diplas & Akiyama (1983) examined the bend equation for finite-amplitude

FIGURE 1. Meander bends on the Pembina River, Alberta, Canada. Flow is from left to right.

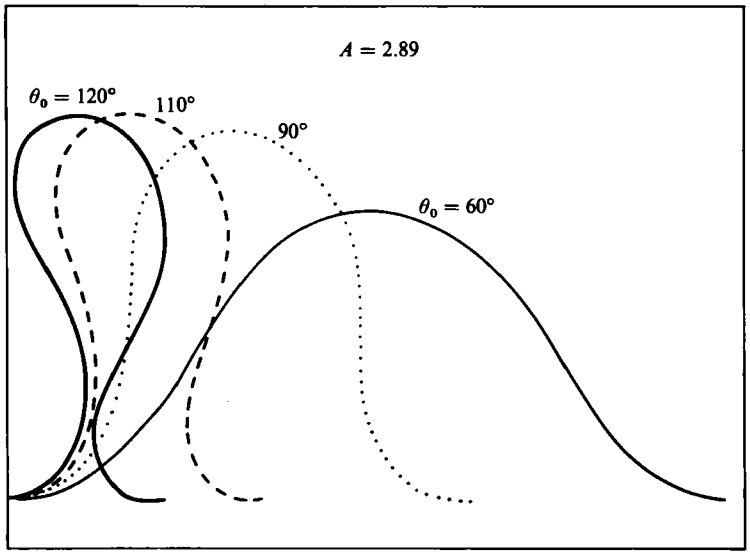

FIGURE 2. Family of periodic solutions of permanent form obtained to third order. Flow is from left to right.

solutions of permanent form. An equation rather similar to that of the Van der Pol oscillator was found to govern such solutions. The family of solutions, shown in figure 2, is remarkably reminiscent of the shape of many high-amplitude bends in nature (e.g. figure 1; see Nanson & Hickin 1983).

The discovery of solutions of permanent form appeared to lend support to previous speculations that there existed some finite-amplitude state to which bend trains tended in the absence of obstructions (e.g. Jefferson 1902). Once this state was reached, bends would migrate downstream without changing amplitude. It is the purpose of the present analysis to show that the solutions of permanent form are in fact unstable.

The analysis applies only to the simplified case of periodic bend trains. It is shown that the ultimate fate of bends of sufficiently long wavelength is cutoff, and that the ultimate fate of bends of sufficiently short wavelength is obliteration by straightening. As a bend train deforms, however, the predicted shape is found to be essentially that of the solutions of permanent form; only the wavenumber differs.

Herein water discharge is assumed to be constant, with the flow maintained at bankfull discharge.

2. Flow mechanics; bank erosion and deposition

A complete discussion of the governing equations is found in Ikeda *et al.* (1981). Centreline values of water-surface slope I, vertically averaged downstream velocity U, and depth H are allowed to vary in time as sinuosity increases, but not in the downstream direction. U, H, and I are constrained by the relations

$$C_f U^2 = gHI, \quad UH = q, \tag{1}$$

where C_f is a friction factor and q denotes water discharge per unit width; both are taken to be constant. Sinuosity S is the average of the ratio of centreline arc length

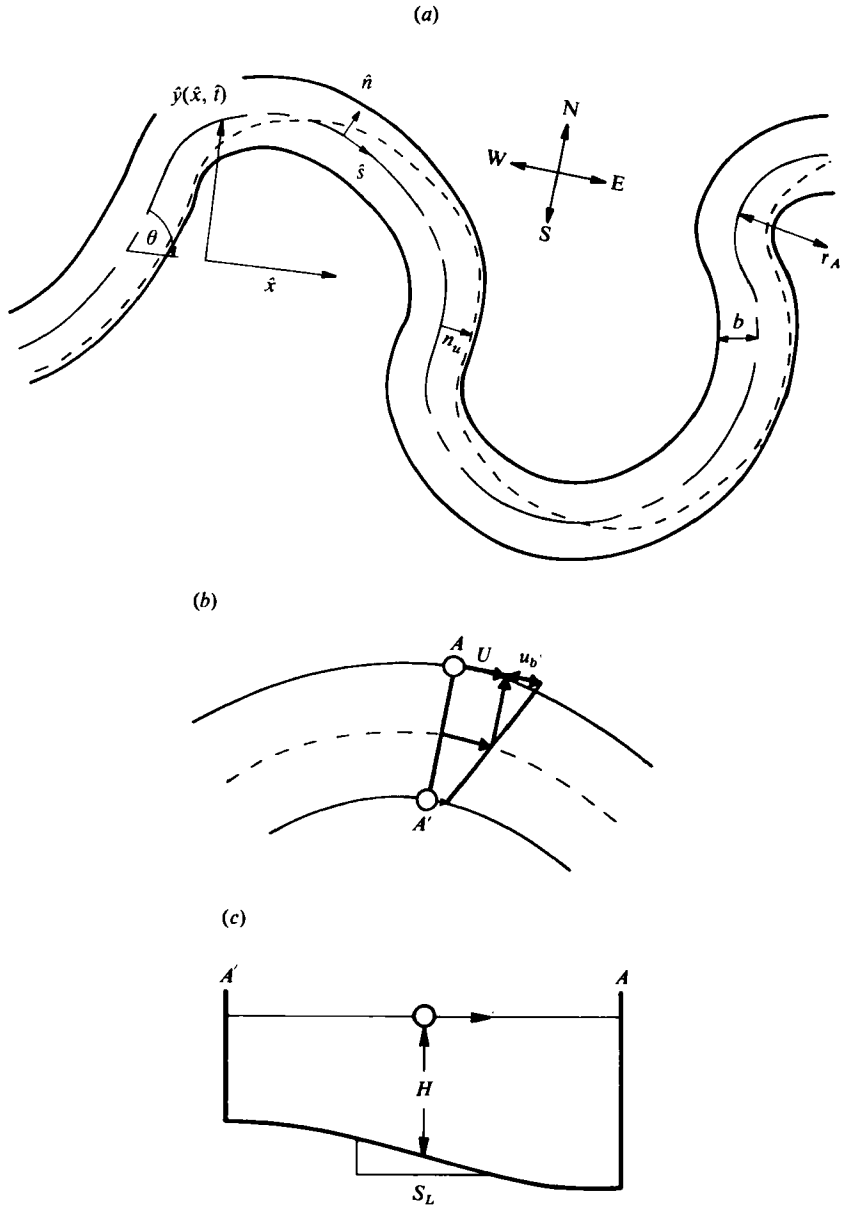

FIGURE 3. (*a*) ——, banks; — — —, centreline; – – – –, locus of high velocity. (*b*) Definition diagram for the downstream velocity profile. (*c*) Definition diagram for channel cross-section.

to downvalley length; on geometric grounds, then,

$$S = \overline{(\cos\theta)^{-1}}, \quad \frac{I}{I_0} = \frac{1}{S}, \tag{2}$$

where the overbar denotes averaging over one wavelength, and channel centreline deflection angle θ is defined in figure 3 (*a*). Defining a dimensionless centreline velocity $\chi = U/U_0$, it is seen from (1) and (2) that

$$\chi = S^{-\frac{1}{3}} = (\overline{(\cos\theta)^{-1}})^{\frac{1}{3}}. \tag{3}$$

As shown in figure 3(*a*, *b*), vertically averaged downstream velocity is assumed to be linear in the normal ($\hat{n}$) direction, given by $U+u_b n_*$, where u_b denotes the difference between the downstream velocity near the left bank looking downstream ('north' bank in figure 3*a*) and the centreline velocity, and $n_* = \hat{n}/b$, where b is the channel half-width. In dimensionless form, this becomes $\chi+un_*$, where $u = u_b/U_0$. The physical significance of such a distribution can be seen by defining the normal coordinate of a locus of high velocity:

$$n_u = \frac{\int_{-1}^{1} n_*(\chi+un_*)\,\mathrm{d}n_*}{\int_{-1}^{1} (\chi+un_*)\,\mathrm{d}n_*} = \frac{1}{3}\frac{u}{\chi}. \tag{4}$$

In figure 3(*a*), the locus of high velocity leans against either the 'north' bank ($n_u > 0$) or the south bank ($n_u < 0$), according to whether u is positive or negative.

The following equation for u can be deduced:

$$\frac{\partial u}{\partial s}+2C_f u = b^*\left[-\chi\frac{\partial C}{\partial s}+C_f(F^2\chi^5+A\chi^2)C\right], \tag{5}$$

where $s = \hat{s}/H_0$ denotes dimensionless centreline arc length, $b^* = b/H_0$, and the dimensionless channel centreline curvature is $C = H_0/r_0$, where r_0 is the centreline radius of curvature (see figure 3*a*); by definition,

$$C = -\frac{\partial\theta}{\partial s}. \tag{6}$$

Also $F = U_0/\sqrt{(gH_0)}$ denotes the Froude number, and A is a dimensionless scour factor given by

$$A = \frac{r_0}{H}S_L, \tag{7}$$

where S_L denotes the local lateral bed slope (figure 3*c*). In general A is of order unity; it increases with U (Kikkawa, Ikeda & Kitagawa 1976; Zimmerman & Kennedy 1978; Odgaard 1981) and thus changes with time. The details of the time variation are unimportant for the present analysis, however, so various constants are used.

For typical values of A ($2 \sim 15$) and Froude numbers less than 0.5, the term containing F in (5) can be dropped; this is done herein.

Ikeda *et al.* (1981) treated bank erosion as follows. Let $\hat{\zeta}$ denote speed of normal channel shift, and let $\zeta = \hat{\zeta}/U_0$; it is assumed that

$$\zeta = E_0 u, \tag{8}$$

where E_0 is a coefficient of bank erosion. Parker (1982) and Beck (1983*a*) have found values of E_0 based on bankfull flow ranging from 8.0×10^{-8} to 3.5×10^{-7} for reaches of the Minnesota River, USA, and the Pembina River, Canada.

Between (4) and (8), it is seen that

$$\zeta = 3\chi E_0 n_u.$$

The channel centreline can be represented as a series of Lagrangian points (figure 4). The above equation defines an orthogonal mapping shown in figure 4, according to which each point in the channel is shifted normal to the centreline an amount proportional to the normal coordinate of the locus of high velocity n_u. This mapping defines the migration evidenced by the scroll bars visible in figure 1, and their orthogonals (Hickin 1974).

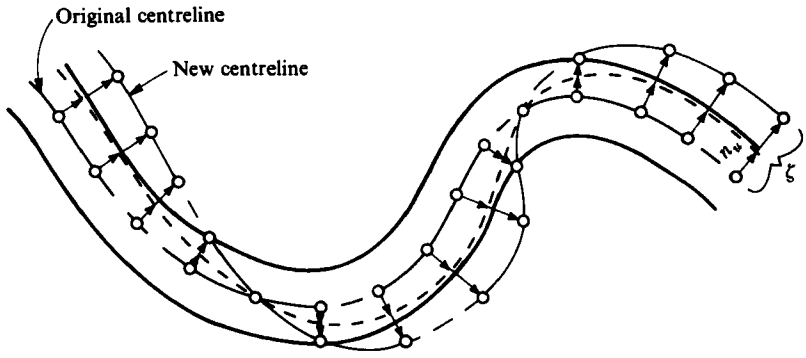

FIGURE 4. Illustration of the use of the orthogonal mapping to compute channel migration. ——, banks; — — —, centreline; - - - -, locus of high velocity.

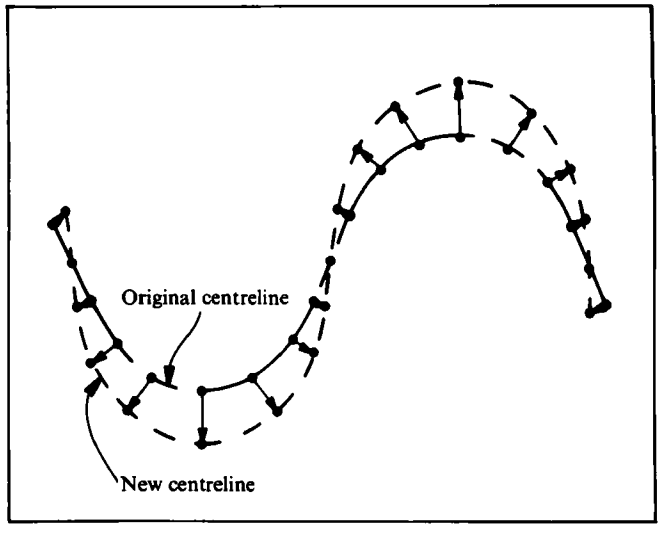

FIGURE 5. Channel migration as predicted by the algebraic relation (12a). Note that no downstream migration is realized.

3. Observations on the mechanism of channel shifting

A reduction of (5) and (8) yields the result

$$\zeta = \int_{\infty}^{s} f(s-s')\, C^*(s')\, \mathrm{d}s', \tag{9}$$

where

$$C^* = \frac{b}{H_0}\, C = \frac{b}{r_0} \tag{10}$$

and

$$f(s) = E_0[-\chi\delta(s) + C_f(A+2)\,\chi^2\, \mathrm{e}^{-2\chi C_f s}], \tag{11}$$

and $\delta(s)$ denotes the Dirac function. The implication of (9) is that the rate of channel shift is linearly proportional to curvature C^*, and influenced by channel shape at all points upstream. The term involving the Dirac function represents a free-vortex effect, which drives the locus of high velocity toward the inner bank; the term involving C_f denotes the effect of friction, which cumulatively drives the locus of high

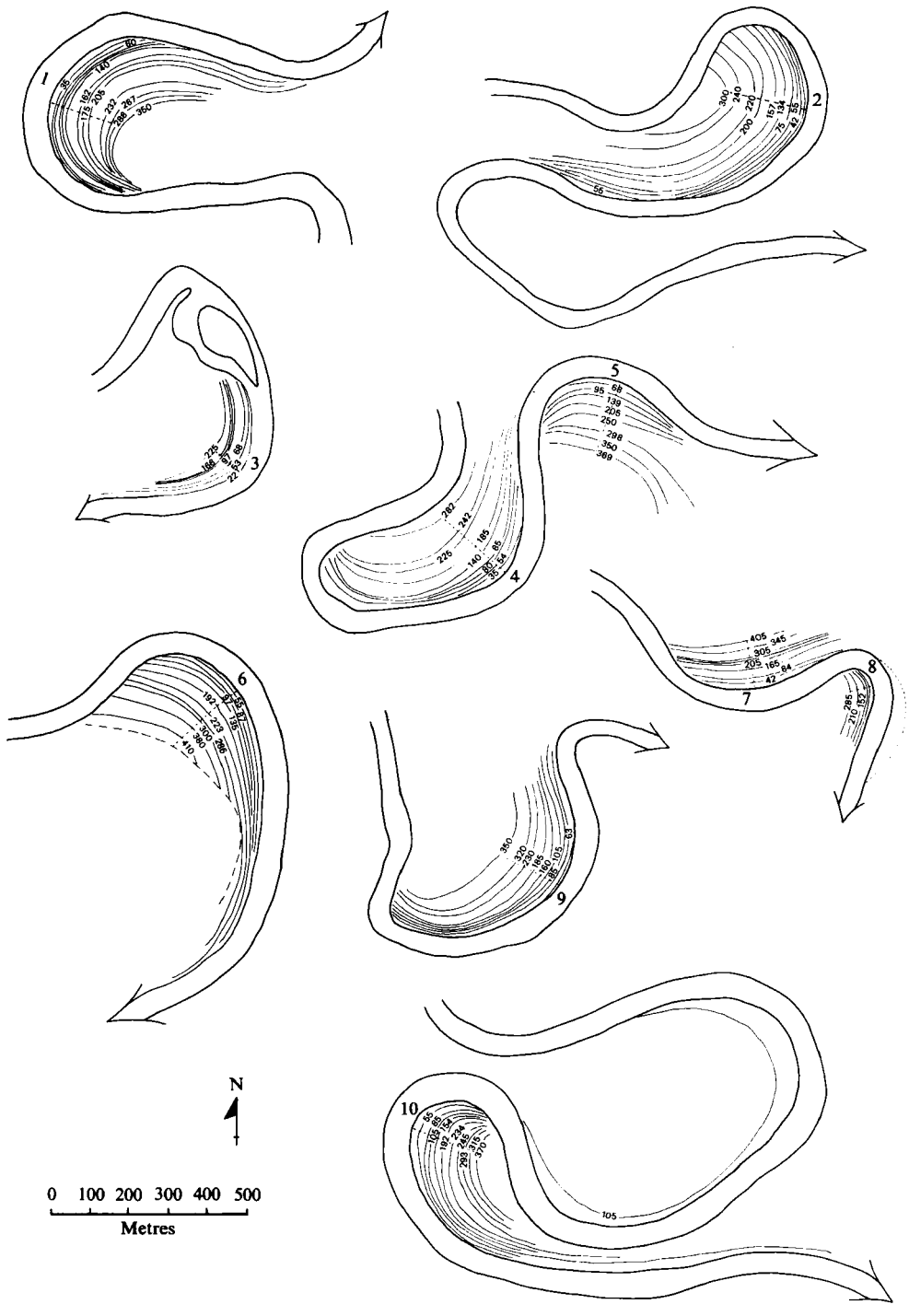

FIGURE 6. Examples of channel migration on the Beatton River, British Columbia, Canada. The numbers on the point bars indicate estimates of the time for formation of scroll bars, in years elapsed from the time of formation to the time of measurement. From Hickin & Nanson (1975); courtesy E. J. Hickin.

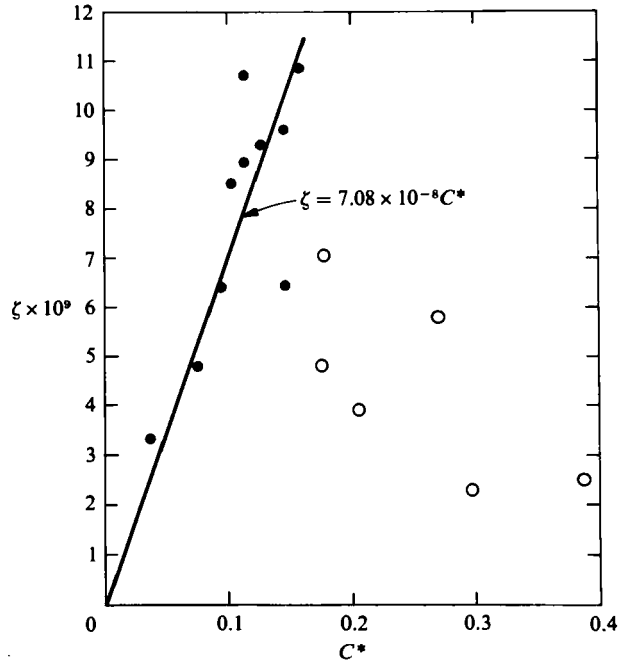

FIGURE 7. Plot of ζ versus C^* for bends of the Beatton River, Canada. Open circles denote points for which $C^* > 0.16$.

Parameter	Value	Parameter	Value
b	35 m	I_0	0.000666
U	1.56 m/s	A	10
H	2.98 m	C_f	0.00360
I	0.0003	F	0.431
S	2.22	k_c	0.0161
χ	0.767	b^*	15.3
U_0	2.04 m/s	E_0	1.85×10^{-8}
H_0	2.28 m		

TABLE 1. Estimates of characteristic parameters at bankfull flow for the Beatton River, Canada

velocity toward the outer bank. Previously Howard & Knutson (1984) have used a convolutional form similar to (9).

Hickin & Nanson (1975) have proposed the local relationship

$$\zeta = f(C^*), \tag{12a}$$

based on scroll-bar spacing from the Beatton River, Canada. As is illustrated in figure 5, (12a) cannot predict downstream migration of the bend pattern. The failure is particularly apparent from the upstream inflection point to near the apex of a given bend. This region, however, tends to obliterate its own scroll bars, and is thus outside of the scope of the treatment of Hickin & Nanson (1975).

From the apex to the downstream inflection point, a tendency toward developed bend flow is realized. This region also leaves the best scroll bars (figure 6), providing the raw material for the analysis of Hickin & Nanson (1975). For developed bend

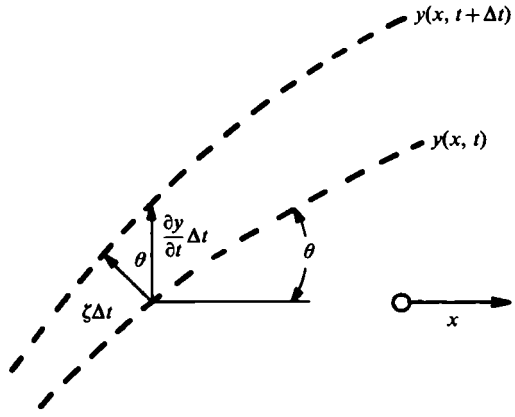

FIGURE 8. Definition diagram for the derivation of (13).

flow with constant curvature, (9) and (11) reduce to

$$\zeta = \tfrac{1}{2}E_0 A\chi C^*. \tag{12b}$$

On figure 7, ζ is plotted against C^* for the data of Nanson & Hickin (1983), using information contained in Hickin & Nanson (1975) and Nanson (1977). Various measured parameters, including A and χ, are given in table 1. It is seen that, for $C^* < 0.16$, ζ is linearly related to C^*, with a coefficient of 7.08×10^{-8}. That is, (12*b*) is found to be accurate for appropriately small curvatures if E_0 takes the value 1.85×10^{-8}.

For value $C^* > 0.16$, figure 7 indicates that ζ decreases rapidly, deviating from (12). This may be due to the fact that the deviation leading to (12) is valid only for small C^*.

4. The bend equation

Let $\hat{x}$ and $\hat{y}$ denote, respectively, downvalley and crossvalley Cartesian coordinates (figure 3*a*), and $\hat{t}$ denote time; the corresponding dimensionless forms x, y and t are formed using the scales H_0 and U_0. It is seen from figure 8 that

$$\zeta = \cos\theta \frac{\partial y}{\partial t}. \tag{13}$$

Also, on geometric grounds,

$$\frac{\partial}{\partial s} = \cos\theta \frac{\partial}{\partial x}, \quad \frac{\partial y}{\partial t} = \int \frac{\partial}{\partial t}(\tan\theta)\,\mathrm{d}x. \tag{14}$$

Thus (5), (8), (13), and (14) reduce to the bend equation,

$$\frac{\partial}{\partial x}\cos\theta \int \frac{\partial}{\partial t}(\tan\theta)\,\mathrm{d}x + 2\chi C_\mathrm{f} \int \frac{\partial}{\partial t}(\tan\theta)\,\mathrm{d}x - \chi \frac{\partial}{\partial x}\left(\cos\theta \frac{\partial\theta}{\partial x}\right) + A\chi^2 C_\mathrm{f} \frac{\partial\theta}{\partial x} = 0, \tag{15}$$

where χ is related to θ via (3).

5. Solutions of permanent form

The linear stability analysis of (15) performed by Ikeda *et al.* (1981) indicates that all infinitesimal disturbances propagate downstream. Let λ denote the Cartesian wavelength of a sinusoidal disturbance, and $k = 2\pi H_0/\lambda$ denote the dimensionless Cartesian wavenumber; it is found that disturbances are stable if $k > k_c$ and unstable if $k < k_c$, where

$$k_c = \sqrt{(2A)}\, C_f. \tag{16}$$

If $\hat{c}$ is the downstream migration speed of the disturbance, and $c = \hat{c}/U_0$, then at $k = k_c$ it is found that $c = c_c$, where

$$c_c = AC_f. \tag{17}$$

Parker *et al.* (1983) showed that (15) admits periodic solutions that migrate downstream at constant speed without changing form. In particular, if (15) is subjected to the transformation

$$x_* = x - ct, \quad t_* = t,$$

assumed to be independent of t_*, and then transformed to intrinsic coordinates, it is found that

$$\chi \frac{d^2\theta}{ds^2} + (c\cos\theta - A\chi^2 C_f)\frac{d\theta}{ds} + 2\chi C_f c \sin\theta = 0. \tag{18}$$

Parker *et al.* (1983) used a Stokesian expansion to obtain a third-order analytical solution to (18). Let λ_a denote arc meander wavelength, and $\kappa = 2\pi H_0/\lambda_a$ denote the dimensionless arc wavenumber. They found the following results: where θ_0 is an angle amplitude taken to be small,

$$\theta = \theta_0 \sin\phi + \theta_0^3\left[\tfrac{1}{192}\sin 3\phi + \frac{\sqrt{(2A)}}{128}\cos 3\phi\right], \tag{19}$$

where $\phi = \kappa s$, and

$$\kappa = k_c(1 - \tfrac{1}{12}\theta_0^2), \quad c = c_c(1 - \tfrac{1}{24}\theta_0^2). \tag{20}$$

From the geometric relationship $k = S\kappa$ and (2), it is found that

$$S = 1 + \tfrac{1}{4}\theta_0^2, \quad k = k_c(1 + \tfrac{1}{6}\theta_0^2). \tag{21}$$

The family of solutions given by (19) are plotted in figure 2 for the value $A = 2.89$ suggested as typical by Ikeda *et al.* (1981). It is readily seen that the solutions are skewed in a fashion reminiscent of figures 1 and 6. Parker *et al.* (1983) termed (19) the Kinoshita curve.

6. Time development of finite-amplitude bends

Parker *et al.* (1983) have shown that the class of solutions represented by (19) resembles actual finite-amplitude bends in many respects. The solutions represent, however, an equilibrium state that may or may not be stable. If this state is stable, as is illustrated in figure 9(*a*), then it can be expected that there is a limit to bend growth before cutoff. In the absence of such random disturbances as varying floodplain erodibility and varying discharge, bends would grow in time to a specific amplitude, and thence migrate downstream without changing form.

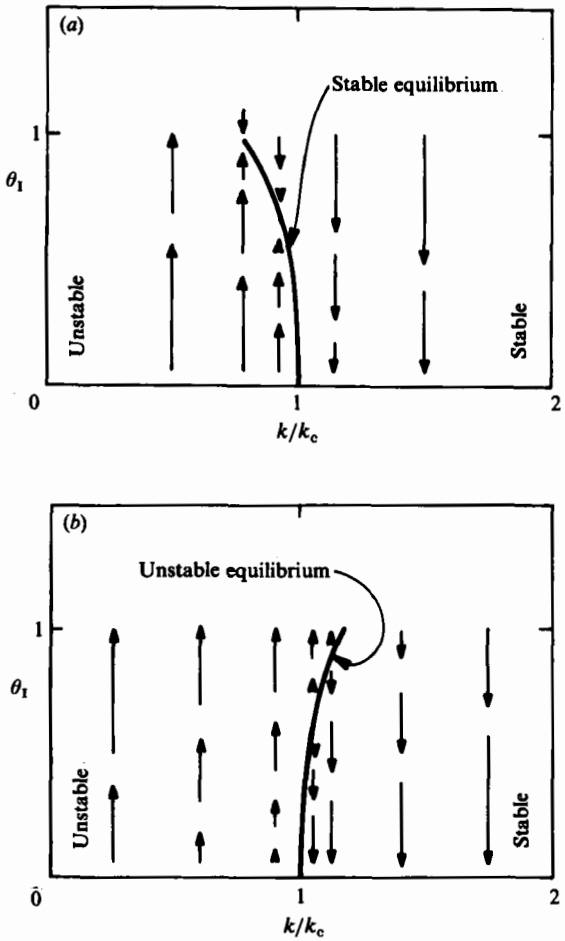

FIGURE 9. (*a*) Hypothetical stability diagram for which certain infinitesimal unstable waveforms would eventually reach finite-amplitude state of permanent form without cutoff. (*b*) Actual stability diagram for the bend equation. The equilibrium, which follows (42*c*), is unstable. All initially unstable bends are eventually cut off.

Herein, however, it is shown that the solution (19) is not stable. At least to third order, the actual situation is as represented in figure 9(*b*).

The method employed is that of two-time expansion in the vicinity of the point of neutral infinitesimal stability (Nayfeh 1973). Let θ_I denote an initial-angle amplitude, again assumed to be small. Then in (15), θ is expanded to third order as

$$\theta = \theta_I \mu_1(\phi, \tau_0, \tau_2) + \theta_I^3 \mu_3(\phi, \tau_0, \tau_2), \tag{22}$$

where

$$\tau_0 = t, \quad \tau_2 = \theta_I^2 t, \tag{23}$$

represent 'fast' and 'slow' timescales, respectively, and

$$\phi = kx, \tag{24}$$

where

$$k = k_c(1 - \beta\theta_I^2). \tag{25}$$

The parameter β is constrained to be of order unity. Note that $\beta > 0$ for infinitesimally unstable bends ($k < k_c$).

Inserting (22)–(25) into (15) and reducing with the aid of (3), the following results are obtained:

$$o(\theta_{\rm I}): \quad k_{\rm c}\frac{\partial^2\mu_1}{\partial\phi\,\partial\tau_0}+2C_{\rm f}\frac{\partial\mu_1}{\partial\tau_0}-k_{\rm c}^3\frac{\partial^3\mu_1}{\partial\phi^3}+C_{\rm f}k_{\rm c}^2A\frac{\partial^2\mu_1}{\partial\phi^2}=0, \tag{26}$$

$$\begin{aligned} o(\theta_{\rm I}^3): \quad & k_{\rm c}\frac{\partial^2\mu_3}{\partial\phi\,\partial\tau_0}+2C_{\rm f}\frac{\partial\mu_3}{\partial\tau_0}-k_{\rm c}^3\frac{\partial^3\mu_3}{\partial\phi^3}+C_{\rm f}k_{\rm c}^2A\frac{\partial^2\mu_3}{\partial\phi^2} \\ & =-k_{\rm c}\frac{\partial^2\mu_1}{\partial\tau_2\,\partial\phi}-\tfrac{1}{2}k_{\rm c}\frac{\partial}{\partial\phi}\left(\mu_1^2\frac{\partial\mu_1}{\partial\tau_0}\right)+\tfrac{1}{2}k_{\rm c}\frac{\partial}{\partial\phi}\left[\left(\int\frac{\partial\mu_1}{\partial\tau_0}\,{\rm d}\phi\right)\frac{\partial}{\partial\phi}\mu_1^2\right] \\ & \quad -2C_{\rm f}\frac{\partial\mu_1}{\partial\tau_2}-2C_{\rm f}\mu_1^2\frac{\partial\mu_1}{\partial\tau_0}+C_{\rm f}(\tfrac{1}{3}\overline{\mu_1^2}-2\beta)\frac{\partial\mu_1}{\partial\tau_0}-\tfrac{1}{2}k_{\rm c}^3\frac{\partial^2}{\partial\phi^2}\left(\mu_1^2\frac{\partial\mu_1}{\partial\phi}\right) \\ & \quad -k_{\rm c}^3(2\beta+\tfrac{1}{6}\overline{\mu_1^2})\frac{\partial^3\mu_1}{\partial\phi^3}+C_{\rm f}k_{\rm c}\beta A\frac{\partial\mu_1}{\partial\phi}+\tfrac{1}{3}C_{\rm f}k_{\rm c}A\overline{\mu_1^2}\frac{\partial\mu_1}{\partial\phi}. \end{aligned} \tag{27}$$

Again, the overbar denotes averaging over one wavelength.

Equations (26) and (27) can be solved using the derivative-expansion procedure outlined in Nayfeh (1973). After considerable algebra, it is found that

$$\theta(x,t)=\theta_{\rm I}\mu_1+\theta_{\rm I}^3\mu_3, \tag{28}$$

where

$$\mu_1=a(\tau_2)\sin(\phi-k_{\rm c}c_{\rm c}\tau_0+b(\tau_2)), \tag{29a}$$

$$\mu_3=\frac{a^2}{192}\left[-11\sin 3(\phi-k_{\rm c}c_{\rm c}\tau_0+b(\tau_2))+3\frac{c_{\rm c}}{k_{\rm c}}\cos 3(\phi-k_{\rm c}c_{\rm c}\tau_0+b(\tau_2))\right], \tag{29b}$$

and

$$\frac{{\rm d}a}{{\rm d}\tau_2}=\frac{k_{\rm c}^2A}{1+\frac{1}{2}A}(\beta a+\tfrac{1}{8}a^3), \tag{30}$$

$$\frac{{\rm d}b}{{\rm d}\tau_2}=c_{\rm c}k_{\rm c}\left\{\beta+\frac{1}{1+\frac{1}{2}A}\left[2\beta+\frac{a^2}{48}(A+18)\right]\right\}. \tag{31}$$

An expression for dimensionless downstream migration speed c can be obtained to order $\theta_{\rm I}^2$ as follows. Let

$$\psi=\phi-k_{\rm c}c_{\rm c}\tau_0+b(\tau_2) \tag{32}$$

denote the total phase in (29a) and (29b). By definition,

$$c=-\frac{1}{k}\frac{\partial\psi}{\partial t}=-\frac{1}{k_{\rm c}(1-\beta\theta_{\rm I}^2)}\left[\frac{\partial\psi}{\partial\tau_0}+\theta_{\rm I}^2\frac{\partial\psi}{\partial\tau_2}\right]. \tag{33}$$

Substituting (32) into (33) and reducing with the aid of (31), it is found that

$$c(\tau_2)=c_{\rm c}\left\{1-\frac{\theta_{\rm I}^2}{1+\frac{1}{2}A}\left[2\beta+\frac{a^2}{48}(A+18)\right]\right\}. \tag{34}$$

The boundary condition on (30) is chosen so that $\mu_1=1$ at $t=0$, i.e. so that the initial angle amplitude of the lowest-order term in (28) is indeed $\theta_{\rm I}$. It follows from (28) and (29a) that

$$a(0)=1. \tag{35}$$

7. Nonlinear stability analysis

Equations (28), (29*a*) and (29*b*) can be transformed into intrinsic coordinates; with the aid of (14), (16) and (17), it is found that

$$\theta = \theta_{\rm I} a \sin(\kappa s - k_{\rm c} c_{\rm c} \tau_0 + b(\tau_2)) + \theta_{\rm I}^3 a^3 \left[\tfrac{1}{192} \sin 3(\kappa s - k_{\rm c} c_{\rm c} \tau_0 + b(\tau_2)) + \frac{(2A)^{\frac{1}{2}}}{128} \cos 3(\kappa s - k_{\rm c} c_{\rm c} \tau_0 + b(\tau_2)) \right], \quad (36)$$

where

$$\kappa = k_{\rm c}[1 - \theta_{\rm I}^2(\beta + \tfrac{1}{4}a^2)]. \quad (37)$$

A comparison of (19) and (36) indicates that as bends develop in time, they take the same form as the equilibrium solutions, regardless of whether those solutions are stable. The only difference is that k is free to differ from the equilibrium value satisfying (21).

Indeed, the equilibrium solution is recovered by setting $\mathrm{d}a/\mathrm{d}\tau_2$ equal to zero in (30). It follows from (30) that, if $a = a_0$ and $\theta = \theta_{\rm I} a_0 \equiv \theta_0$ at equilibrium,

$$\beta = -\tfrac{1}{6}a_0^2. \quad (38)$$

A substitution of this result into (25) and (34) yields (20) and (21), so the equilibrium solution is completely recovered. Since initially $a(0) = 1$, it follows that a bend with a wavelength such that

$$\beta = -\tfrac{1}{6}, \quad (39)$$

maintains permanent form subsequently.

The stability of this permanent form is governed by (30). The solution to (30) and (35) is

$$a^2 = \frac{\beta \, \mathrm{e}^{12\beta\tau_{\rm r}}}{\beta + \frac{1}{6}(1 - \mathrm{e}^{12\beta\tau_{\rm r}})}, \quad (40)$$

where

$$\tau_{\rm r} = \frac{k_{\rm c}^2 A}{6(1 + \frac{1}{2}A)} \tau_2. \quad (41)$$

The following can be easily verified from (40). If $\beta < -\frac{1}{6}$, or from (25)

$$k > k_{\rm c}(1 + \tfrac{1}{6}\theta_{\rm I}^2), \quad (42a)$$

then all bends subside to the straight state. If, on the other hand, $\beta > -\frac{1}{6}$, or

$$k < k_{\rm c}(1 + \tfrac{1}{6}\theta_{\rm I}^2), \quad (42b)$$

then infinite amplitude is reached in a finite amount of time.

The result is schematized in figure 9(*b*). It is seen that the line of equilibrium

$$k = k_{\rm c}(1 + \tfrac{1}{6}\theta_{\rm I}^2) \quad (42c)$$

curves to the right on the $(k, \theta_{\rm I})$-plane, so that the equilibrium state is unstable. Sufficiently short bends are obliterated. Sufficiently long bends continue to grow at a rate that accelerates as angle amplitude (and bend curvature) increases. It is likewise seen from (34) that, for bends that grow in amplitude, the downstream migration rate declines in time.

The above picture is valid only to the extent that the present third-order analysis applies. Beck (1983*b*), however, has confirmed these conclusions via numerical calculations.

In fact, bends do not reach infinite amplitude in a finite amount of time. Rather,

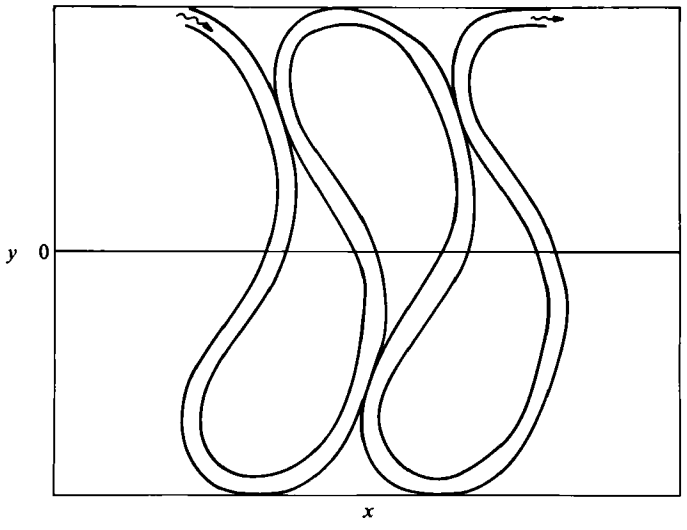

FIGURE 10. Bend shape at incipient neck cutoff ($\theta_0 = 121°$) for $A = 10$.

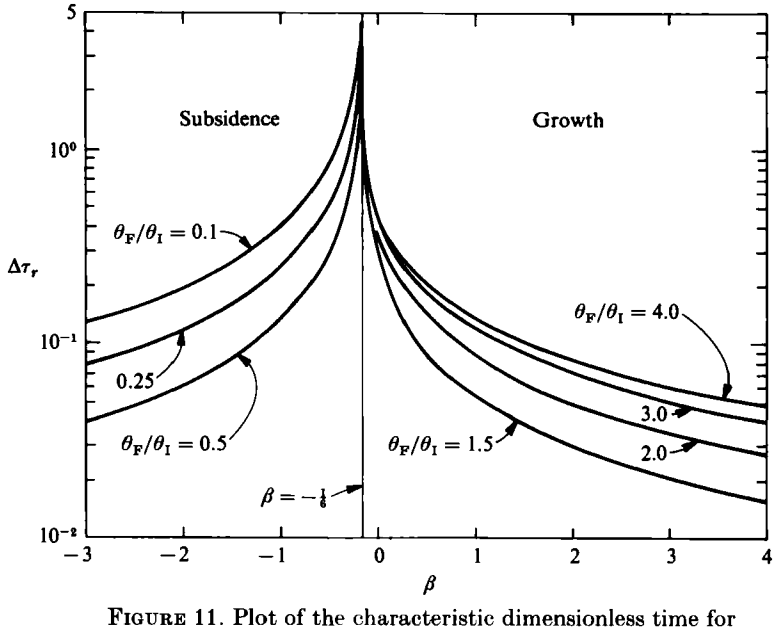

FIGURE 11. Plot of the characteristic dimensionless time for angle amplitude to change from θ_I to θ_F.

they cut off. Assuming a value of 20 for the parameter λ_c/b (Leopold, Wolman & Miller 1964), and a value of 10 for A (appropriate for the Beatton river), it is readily shown the the Kinoshita curve (19) is subject to neck cutoff at an angle of 121°, as shown in figure 10.

Equations (28), (29a), (29b), (40), and (41) can be used to derive a formula for the amount of time required for a bend to increase (decrease) in angle amplitude from an initial value of θ_I to a final value of θ_F; i.e. the time required for the parameter a to change from its initial value of unity to $a = \theta_F/\theta_I$. From (40), the dimensionless

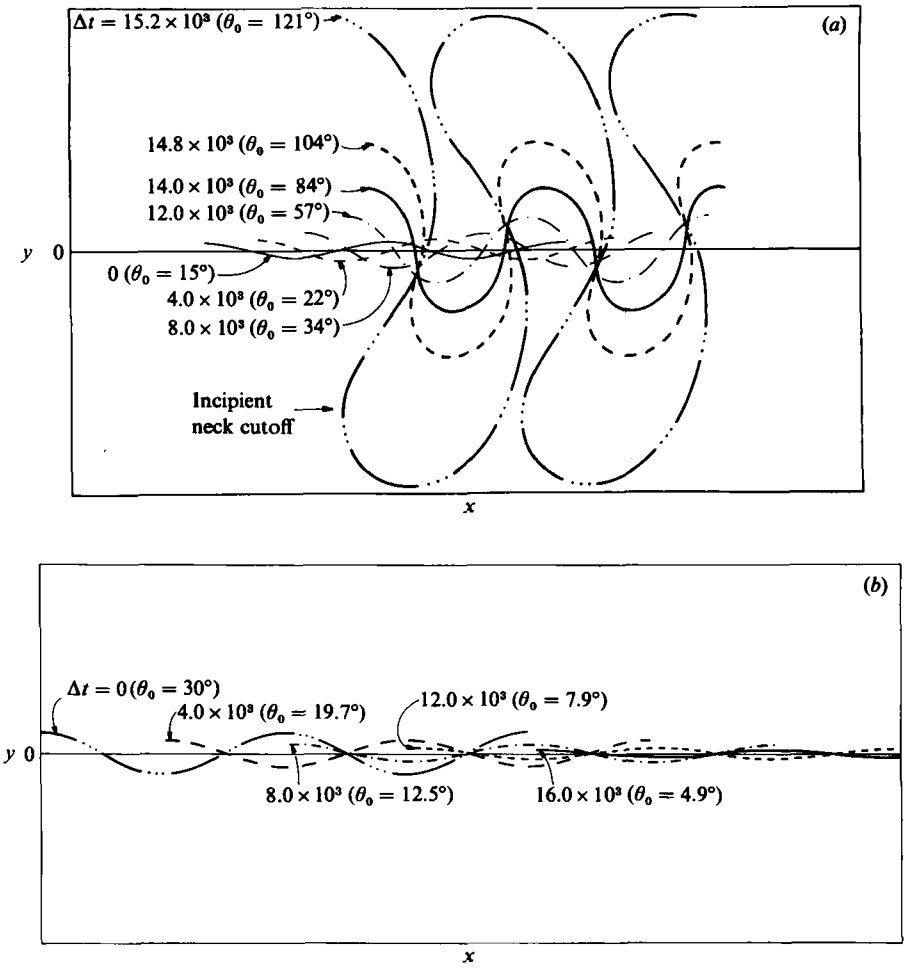

FIGURE 12. (*a*) Time development of an unstable bend, $\theta_I = 15°$. The parameter Δt is defined in (44). (*b*) Time development of a stable bend; $\theta_I = 30°$. The parameter Δt is defined in (44).

time increment $\Delta\tau_r$ is

$$\Delta\tau_r = \frac{1}{12\beta}\ln\left[\frac{(\theta_F/\theta_I)^2(6\beta+1)}{6\beta+(\theta_F/\theta_I)^2}\right]. \tag{43}$$

The required dimensioned time interval $\Delta\hat{t}$ is found to be equal to $H_0\Delta t/(U_0 E_0 b^*)$, where

$$\Delta t = \frac{1+\frac{1}{2}A}{2k_c^2 A\theta_I^2}\frac{1}{\beta}\ln\left[\frac{(\theta_F/\theta_I)^2(6\beta+1)}{6\beta+(\theta_F/\theta_I)^2}\right]. \tag{44}$$

In figure 11, $\Delta\tau_r$ is plotted as a function of β and θ_F/θ_I. Clearly, for bends near the equilibrium state ($\beta = -\frac{1}{6}$), change is very slow. As bends become longer than the equilibrium wavelength (β increases), growth increases in rapidity, as evidenced by declining values of $\Delta\tau_r$.

8. Discussion

For the purpose of providing a fairly typical illustration of the consequences of the theory, values of A and k_c appropriate for the Beatton River are used. From table 1 and (16) it is found that $k_c \approx 0.0161$, corresponding to a critical Cartesian wavelength of 890 m. Recalling that small-amplitude bends must have a longer Cartesian wavelength in order to grow, this value appears to be in the right range for the bends of the Beatton River (figure 6).

In figure 12, the time development of two-bend trains are considered. The first bend has an initial angle amplitude of θ_I of 0.261 (15°), and a wavenumber k equal to $0.794k_c$ ($\beta = 3$). The prediction is carried to cutoff, even though the analysis may not be valid in detail at such a high amplitude. In the case of the second bend, the initial amplitude θ_I is 0.524 (30°), and k is equal to $1.27k_c$ ($\beta = -1$).

The growing bend exhibits a simple shape that is nevertheless reminiscent of the more complicated shapes of figures 1 and 6. The subsiding bend illustrates that the theory can predict deposition on the outside, and erosion on the inside, of short bends. This phenomenon is not seen often, because such bends tend to be self-obliterating. Nevertheless, Woodyer (1975), Hickin (1979), and Reid (1983) have observed such bends.

The present analysis suggests that bends that initially grow continue to do so until cutoff, meanwhile accelerating their growth rate. Indeed, cutoffs are a very prominent feature of the floodplains of meandering streams (figure 1). At cutoff, however, curvature C^* is often sufficiently high to invalidate the present analysis. It may be that an inclusion of terms dropped in deriving (5) would cause the erosion rate to decline (or even reverse) with increasing C^*, so that some bends might not be cut off. Another possibility exists, however, to explain the decline in erosion rate with C^* observed in figure 7 for $C^* > 0.16$. An obstacle such as bedrock, or the interaction of adjacent bends, may cause the Cartesian wavelength of a bend to decrease (so that k increases). This may push the bend from the unstable region into the stable region, as illustrated in figure 9(*b*). The outward erosion rate would decline, and finally reverse. The behaviour is intimately tied up with the form of (9), and cannot in principle be simplified to the form of (12). Reid (1983) in particular has emphasized the role of bedrock in blocking downstream bends on the Connecticut River, forcing them to shorten, and eventually deposit on the outside.

For a typical illustration of the predicted timescale for change, the time required for a bend with θ_I equal to 0.349 (20°) to double in amplitude is computed from (44). A value of β of 4 is used; other parameters are those estimated for the Beatton River in table 1. It is found that 378 years is required for a doubling in amplitude, a value in general accord with the scrollbar dates on figure 6.

9. Conclusion

The method of the two-time expansion is applied to the bend equation of Ikeda *et al.* (1983) in order to study the time development of periodic meander bend trains. The equilibrium family of solutions delineated by Parker *et al.* (1983) is found to be unstable. According to the analysis, bends with a sufficiently long Cartesian wavelength grow until cutoff, and sufficiently short bends return to the straight state. The analysis is carried only to the third order; numerical studies by Beck (1983*b*) on the bend equation, however, confirm the above conclusions.

Both bend shape and the predicted rate of shifting appear to be in general accord

with the field observations of Hickin & Nanson (1975) and Nanson & Hickin (1983).

The bend equation is applicable to arbitrary amplitude, but the ratio of channel half-width to centreline radius of curvature must be modest. Short, sharp bends are often characterized by declining rates of outward migration, or even a reversal of the direction of migration. This behaviour may be due to curvature terms dropped in the derivation of the bend equation. It may also be associated with decrease in Cartesian wavelength due to, for example, an obstacle inhibiting downstream migration. The latter mechanism of stabilization can be explained qualitatively in the context of the present analysis.

Certain criticisms are in order. The bend equation is based on Engelund's (1974) treatment of bend flow. This simplified model possesses certain defects discussed by Smith & McLean (1985), and Blondeaux & Seminara (1985). Only constant flows and floodplains of erodibility are considered. The analysis is accurate only for a rather modest range of wavenumbers near the critical value. The interaction of non-periodic bends is not treated.

Much of the above-mentioned research was performed during the first author's annual summer tenure as a research hydrologist with the US Geological Survey. The research was supported by the National Science Foundation (Grant CEE8204953 and CEE8311721), and the Legislative Committee on Minnesota Resources.

REFERENCES

Beck, S. M. 1983*a* Lateral Channel Stability of the Pembina River near Rossington, Canada. Research Council of Alberta, Edmonton, Alberta, Canada.

Beck, S. M. 1983*b* Mathematical modeling of meander interaction. In *Proceedings, Rivers, '83 Specialty Conference on River Meandering, ASCE*, October 24–26, New Orleans, USA, 932–941.

Blondeaux, P. & Seminara, G. 1985 A unified bar–bend theory of river meanders. *J. Fluid Mech.* **157**, 449–470.

Carson, M. A. & Lapointe, M. F. 1983 The inherent asymmetry of river meander planform. *J. Geol.* **91**, 41–55.

Engelund, F. 1974 Flow and bed topography in channel bends. *J. Hydraul. Div. ASCE* **100**, 1631–1648.

Hickin, E. J. 1974 The development of meanders in natural river-channels. *America Journal of Science* **274**, 414–442.

Hickin, E. J. 1979 Concave-bank benches on the Squamish River, British Columbia, Canada. *Can. J. Earth Sci.* **16**, 200–203.

Hickin, E. J. & Nanson, G. C. 1975 The character of channel migration on the Beatton River, Northeast British Columbia, Canada. *Geol. Soc. Am. Bull.* **86**, 487–494.

Hooke, R. LeB. 1975 Distribution of sediment transport and shear stress in a meander bend. *J. Ecology* **83**, 543–565.

Howard, A. D. & Knutson, T. R. 1985 Sufficient conditions for river meandering: a simulation approach. *Water Resources Res.* (In the Press.)

Ikeda, S., Parker, G. & Sawai, K. 1981 Bend theory of river meanders. 1. Linear development. *J. Fluid Mech.* **112**, 363–377.

Jefferson, M. 1902 The limiting width of meander belts. *Natl Geog. Mag.* **13**, 373–384.

Kikkawa, H., Ikeda, S. & Kitagawa, A. 1976 Flow and bed topography in curved open channels. *J. Hydraul. Div. ASCE* **102**, 1327–1342.

Kinoshita, R. 1961 *An Investigation of Channel Deformation of the Ishikari River.* Publication no. 36, Natural Resources Division, Ministry of Science and Technology of Japan, 139 pp. (in Japanese).

Kitanidis, P. K. & Kennedy, J. F. 1984 Secondary current and river-meander formation. *J. Fluid Mech.* **144**, 217–230.

LEOPOLD, L. B., WOLMAN, M. G. & MILLER, J. P. 1964 *Fluvial Processes in Geomorphology*. San Francisco: W. H. Freeman. 522 pp.

NANSON, G. C. 1977 Channel migration, floodplain formation, and vegetation succession on a meandering-river floodplain in N.E. British Columbia, Canada. Ph.D. thesis, Simon Fraser University, British Columbia, Canada. 349 pp.

NANSON, G. C. & HICKIN, E. J. 1983 Channel migration and incision on the Beatton River. *J. Hydraul. Div. ASCE* **109**, 327–337.

NAYFEH, A. 1973 *Perturbation Methods*. John Wiley.

ODGAARD, A. J. 1981 Transverse bed slope in alluvial channel bends. *J. Hydraul. Div. ASCE* **107**, 1677–1694.

PARKER, G. 1982 Stability of the channel of the Minnesota River near State Bridge No. 93, Minnesota. Project Report No. 205, St Anthony Falls Hydraulic Laboratory, University of Minnesota, USA, 33 pp.

PARKER, G., SAWAI, K. & IKEDA, S. 1982 Bend theory of river meanders. Part 2. Nonlinear deformation of finite-amplitude bends. *J. Fluid Mech.* **115**, 303–314.

PARKER, G., DIPLAS, P. & AKIYAMA, J. 1983 Meander bends of high amplitude. *J. Hydraul. Div. ASCE* **109**, 00–00.

REID, J. B. 1983 Artificially-induced concave bank deposition as a means of floodplain erosion control. *Proceedings, Rivers, '83 Specialty Conference on River Meandering, ASCE*, October 24–26, New Orleans, USA.

SMITH, J. D. & MCLEAN, S. R. 1985 A model for meandering streams. *Water Resources Res.* (In the Press.)

WOODYER, K. D. 1975 Concave-bank benches on the Barwon River, New South Wales. *Austral. Geographer* **13**, 36–40.

ZIMMERMAN, C. & KENNEDY, J. F. 1978 Transverse bed slopes in curved alluvial channels. *J. Hydraul. Div. ASCE* **104**, 33–48.